Journal of Sea Research 186 (2022) 102242

Contents lists available at ScienceDirect

Journal of Sea Research

journal homepage: www.elsevier.com/locate/seares

Residual circulation and freshwater retention within an event-driven system of intertidal basins

Carmine Donatelli [a,*,1], Matias Duran-Matute [b], Ulf Gräwe [c], Theo Gerkema [a]

[a] NIOZ Royal Netherlands Institute for Sea Research, Department of Estuarine and Delta Systems, Yerseke, the Netherlands
[b] Eindhoven University of Technology, Department of Applied Physics, Eindhoven, the Netherlands
[c] Leibniz-Institute for Baltic Sea Research, Department of Physical Oceanography and Instrumentation, Warnemuende, Germany

ARTICLE INFO

Keywords:
Residual flow
Extreme flushing events
Event-driven systems

ABSTRACT

This study explores the spatiotemporal variability in the residual circulation and its dependence on external forces in an interconnected system of intertidal basins. We focus on the Dutch Wadden Sea (DWS), where winds play a major role in water movements and storms significantly affect its short-term characteristics. We make use of realistic three-dimensional high-resolution numerical simulations to model the hydrodynamics in the DWS for the years 2005–2015. First, the 'empirical orthogonal function' method is applied to analyze systematically the relative contributions of various forcing mechanisms on the residual (i.e., tidally averaged) volume flow through the inlets and the shallow watersheds delimiting the system and each tidal basin. Then, we compute the tidally averaged flushing frequency of fresh water over the entire period of analysis, and we study its variations at short and long time scales. It is found that over 98% of the residual flow's spatiotemporal variations can be explained by the first three EOF modes, which are highly correlated with the cubic power of the vectorial wind components' speed and the amount of fresh water discharged into the back-barrier system. This study reveals that incidental short-duration events (e.g., storms) occurring at time scales of hours to days, albeit episodic and highly variable, strongly influence the residual transport's inter-annual variability and its long-term typical value in multiple-inlet coastal systems.

1. Introduction

The study of the residual circulation (here defined as the circulation resulting from averaging over the oscillatory tidal component of the currents) is critical for the ecology of coastal systems, since it affects the net exchange of suspended sediments, nutrients, larvae and contaminants [e.g., Talke et al., 2009]. The residual volume transport of water through a multiple-inlet coastal system is forced by different drivers such as tides, winds, freshwater discharge and baroclinic effects. For instance, the nonlinear interaction of the tides with the bathymetry and differences in the tidal amplitude (and phase) among the inlets create a residual tidal flow [van de Kreeke and Cotter, 1974; Zimmerman, 1981]. This means that a purely oscillatory tidal current gives rise to a residual signal (i.e., a net current is found after averaging the currents over a tidal cycle) [Gerkema, 2019]. Wind generates a residual flow as well, but given its episodic nature, the effect can vary in direction and intensity over time, making the residual flow extremely variable [e.g., Smith, 1990]. The residual circulation is also important for the freshwater transport, and it is used together with transport time scales to evaluate the freshwater pathways and retention in estuaries and coastal bays [Phelps et al., 2013; Duran-Matute et al., 2014].

Transport time scales (e.g., age, flushing time) are important metrics in coastal environments and are relevant to explain several key ecological and biological processes. Quantifying the rate at which tidal basins flush nutrients and pollutants into the coastal ocean is paramount for management purposes, and it is fundamental to assess the resilience of these systems to natural and anthropogenic threats. Nutrient over-enrichment caused by human activities has degraded many coastal waters worldwide with severe consequences on the aquatic ecology, although the characteristics of this stressor have improved in the last decades [e.g., Philippart et al., 2007; Jung et al., 2017]. Numerous studies document that this issue is linked to a variety of cascading environmental problems (e.g., increase in the micro- and macroalgal growth, harmful algal blooms) resulting in dramatic loss of habitats (e.

* Corresponding author.
E-mail address: carmine.donatelli@nioz.nl (C. Donatelli).
[1] Present Address: Department of Civil, Architectural and Environmental Engineering, University of Texas at Austin, Austin, TX, USA.

https://doi.org/10.1016/j.seares.2022.102242
Received 3 December 2021; Received in revised form 7 June 2022; Accepted 22 June 2022
Available online 28 June 2022

g., seagrasses, salt marshes) [e.g., Kennish, 2001] and related ecosystem services [e.g., Donatelli et al., 2019]. In addition, long retention times of nutrients in poorly flushed estuaries and coastal lagoons further diminish the survival of essential ecosystems [e.g., Nixon et al., 1996; Kemp et al., 2005; Burkholder et al., 2007]. Thus, evaluating water renewal in tidal embayments bears important consequences for the ecology, and it is a critical step to improve water quality and coastal habitat conditions [Jiang et al., 2019].

Three different transport time scales are commonly employed to quantify the efficiency of water renewal in coastal systems: the 'age', the 'residence time' and the 'flushing time' (or 'turn-over time'). Definitions of these transport time scales vary within the literature; here we shall follow Bolin and Rodhe [1973] and Zimmerman [1976] who first introduced these concepts, but for an exhaustive and complete review of the topic, see Takeoka [1984]. The 'age' (τ) represents the time spent by a water parcel within the waterbody of interest since it entered through one of its boundaries up to a certain instant t [Bolin and Rodhe, 1973], whereas the 'residence time' is defined as the time it takes for the water parcel to leave the system through its outlet to the sea from that instant t onward [Zimmerman, 1976]. 'Age' and 'residence time' are complementary concepts and they depend on the spatial location of the water parcel, specification of the domain's boundaries and time of particles' release. In contrast, the 'flushing time' is a bulk or integrative parameter describing the general exchange characteristics of a tidal embayment. Specifically, it estimates the retention of water (or scalar quantities transported with water) in a coastal system, and it is defined in steady-state conditions by the ratio of the total mass of a specific constituent in the waterbody to the outflow [e.g., Officer, 1976]. This definition is not suitable for dynamic systems [Monsen et al., 2002]. Therefore, many authors proposed alternative definitions for computing this transport time scale [e.g., Duran-Matute et al., 2014].

To the best of our knowledge, studies focusing on the role of the wind forcing on the residual circulation in multiple-inlet coastal systems across different time scales are limited [e.g., Li, 2013; Duran-Matute et al., 2016]. Specifically, this paper aims at unraveling the cumulative impact of sporadic short-duration events occurring at time scales of hours to days on its yearly mean (and median) values. To analyze systematically the wind effect on the residual flow, we look at the long-term statistics and then we isolate: (i) periods characterized by calm conditions to estimate the tidally driven residual flow (no wind effects), and (ii) extreme events to reveal whether storms can leave a mark on the long-term residual transport. We address these processes by using a three-dimensional hydrodynamic model and the Dutch Wadden Sea (DWS) as a test case.

The dynamics of the DWS was considered by previous researchers as statistically steady (i.e., driven by the cyclical tides) due to lack of data which included long time spans [e.g., Zimmerman, 1976]. In this view, the wind was conceived merely as a perturbing factor. For instance, Ridderinkhof [1988] employed a numerical model to study the transport in the western part of the DWS, including only tides. Recent outcomes based on high-resolution numerical simulations covering the years 2009–2011 demonstrated that the residual flows and transports in the DWS present a strong temporal variability, chiefly due to winds [Duran-Matute et al., 2016]. Since a period of three years was not sufficient to identify the long-term typical state of the system due to the strong inter-annual variability of the wind, we now increase the time frame of analysis to 11 years which allows us to quantify and understand the relationship between the residual flow among different tidal basins and with the North Sea under a variety of forcing conditions. More specifically, the length of the numerical simulations helps us to define the typical state of the system with respect to which the consequences of anthropogenic interventions and climate change could be estimated. Thus, this study has potential implications for management purposes, and for understanding the ecology of the area and its spatial heterogeneity [e.g., Schwichtenberg et al., 2017].

In the present paper, we aim at determining the impact that winds and storms have, despite their episodic nature, on the long-term residual transport in the Dutch Wadden Sea, and in multiple-inlet coastal systems in general. In addition, we devote particular attention to temporal variations in the system's freshwater retention [e.g., Matsoukis et al., 2021]. The latter depends on the fresh water discharged into the DWS and it is ultimately controlled by the residual freshwater transport at the transects delimiting the system (e.g., tidal inlets, shallow watersheds). In particular, we analyze how the freshwater flushing changes at short and long time scales, and we perform a statistical characterization of the occurrence of extreme flushing events.

These topics have a broad impact given the relevance of the residual transport on the long-term exchange of nutrients and sediments between back-barrier systems and the coastal ocean, and the importance of water renewal on critical biological and biogeochemical processes (e.g., eutrophication, nutrient and phytoplankton concentrations, development of anoxic and hypoxic conditions). Furthermore, identifying the dominant mechanisms controlling the residual circulation across different time scales may help to unravel whether (and how) variations in atmospheric forcing triggered by climate change can alter the character of the dynamics in coastal systems, and subsequent long-term water and material exchanges with the shelf [e.g., Zhang et al., 2020].

The paper is organised as follows. Section 2 describes the study site. The model setup and methods for data analysis are presented in Section 3. In Section 4, the spatiotemporal changes in the residual water volume transport under calm conditions (Subsection 4.1) and considering the wind effect (Subsections 4.2 and 4.3) are analyzed. The study of the freshwater retention is performed in Section 4.4. Finally, the discussion is presented in Section 5 and the conclusions are outlined in Section 6.

2. Study site

The Wadden Sea is the largest system of interconnected tidal flats in the world, and it was listed by UNESCO as a world heritage in 2009. It is located along the coast of the Netherlands, Germany and Denmark. The Dutch part of the Wadden Sea extends from the Texel inlet to the Ems-Dollard estuary, and it is separated from the North Sea by a series of barrier islands. Fig. 1 depicts the DWS between the Texel inlet and the Groninger Wad; the three most westernmost tidal basins of this subregion will be the focus of our study. Several inlets connect the basins with the North Sea (see A to E in Fig. 1). Each tidal basin presents different characteristics in terms of tidal prism, area of intertidal flats

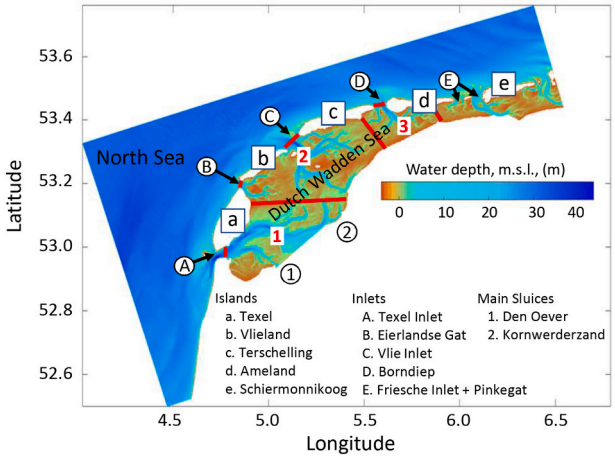

Fig. 1. Study area. Bathymetry of the Dutch Wadden Sea. The red lines represent the transects delimiting the three tidal basins considered in this study. The red lines within the system indicate the three shallow watersheds: Watershed 1 (the westernmost watershed), Watershed 2 and Watershed 3 (easternmost watershed). (For interpretation of the references to colour in this figure legend, the reader is referred to the web version of this article.)

and orientation with respect to the dominant wind [Duran-Matute et al., 2016]. Two main sources of fresh water are present in the system, namely the sluices at Den Oever and Kornwerderzand (see 1 to 2 in Fig. 1). Postma [1950] showed that the fresh water from Den Oever leaves the DWS mainly via Texel Inlet, whereas the fresh water from Kornwerderzand has a more complicated path. Zimmerman [1976] argued that 1/3 of the fresh water coming from Kornwerderzand leaves the system through Texel inlet, while the remaining part is lost to the coastal ocean via the Vlie inlet. Recently, Duran-Matute et al. [2014] showed that the tidal prism alone is not an adequate metric for the water renewal within the basins. For instance, the Vlie has a similar tidal prism as Texel Inlet, but the former involves a much smaller net export of fresh water. In other words, the fresh water merely goes back and forth with the tide without really leaving the basin. By contrast, Texel Inlet is considered a major exit route.

3. Methods

High-resolution numerical simulations were carried out using the General Estuarine Transport Model (GETM) to simulate the hydrodynamics in the Dutch Wadden Sea for the period 2005–2015 (Subsection 3.1). We explore the dependence of the water volume inside the system and residual volume transport on the external forces, notably wind energy, see Subsection 3.2. In particular, the variability of the residual transport is analyzed using the 'empirical orthogonal functions' (EOF) method (Subsection 3.3). The main goal of this method is to extract from the dataset (i.e., time series of the residual transport across different transects) independent patterns by reducing the original time series to few modes of variability. The EOF analysis provides a set of eigenvectors (or 'structure functions'), which are ordered hierarchically according to the eigenvalues. Each eigenvalue explains a certain fraction of the variance in the dataset. The eigenvectors (EOFs) provide information about the spatial structure, whereas the expansion coefficients (ECs) are the amplitudes of these 'structure functions' in time. The ECs give an indication of the temporal variability in the dataset. It is worth noticing that the EOF analysis is based on mathematical principles, and hence, the orthogonal modes have to be interpreted once they are obtained. We use correlation coefficients between the ECs and the external forces (e.g., wind energy, freshwater discharge) to distinguish between 'data modes' and 'physical modes' [Newman and Sardeshmukh, 1995; Zhang et al., 2012]. Furthermore, we calculate the freshwater volume and the flushing frequency (i.e., the reverse of the flushing time) of fresh water to investigate how the retention capacity of the DWS varies over time (Subsection 3.4). The 'peak over threshold' method (Subsection 3.5) is employed to analyze statistically the occurrence of extreme values in the flushing frequency's time series.

3.1. Hydrodynamic model

We simulated the hydrodynamics in the Dutch Wadden Sea with a 3D hydrodynamic model from January 2005 to December 2015, using GETM [Burchard and Bolding, 2002]. The freshwater dispersal in the system was tracked using Eulerian passive tracers, adopting an approach similar to Meier [2007] and Zhang et al. [2009]. Two distinct tracers were employed, one for each freshwater outlet. In this study, we used the framework for Aquatic Biological Modeling (FABM) passive tracer module coupled with GETM, which solves the advection-diffusion equation for the passive tracers employing the same method used for salinity and temperature.

A four-nested grid model was used as in Gräwe et al. [2016]. The DWS' numerical grid has a horizontal resolution of 200 m, and the water column is discretized with 25 layers. Bathymetric data around the year 2009 has been used for the entire period of analysis. The model was earlier calibrated and validated with available observations (see supplementary material) [e.g., Duran-Matute et al., 2014; Gräwe et al., 2016]. We used atmospheric data with a spatial resolution of 6 km and a temporal resolution of 1 h (reanalysis data of COSMO-REA6 [Frank et al., 2018]). Water levels at the numerical domain boundaries were obtained by superimposing astronomic tidal elevations, computed by using the Oregon State University Tidal Prediction Software (OSU-TPS), and surge levels calculated employing a vertically integrated North Atlantic model forced by surface winds and air pressure. Rijkswaterstaat provided time series of freshwater discharges at the main sluices. In addition, we adopted a new routine for the air-sea fluxes based on Kara et al. [2005], whereas previous runs [e.g., Duran-Matute et al., 2014] employed the Kondo [1975] formulation to compute the transfer coefficients. Specifically, Kara et al. [2005] derived a set of expressions for the bulk transfer coefficients having a polynomial dependence on wind speed and a linear dependence on the air-sea temperature difference. A linear dependence on wind speed for computing the exchange coefficients has been shown to be less accurate [Blake, 1991].

3.2. Sectorial wind components and wind energy

We used the wind energy to characterize the wind climate in the study site over the period 2005–2015. The wind direction (*from* which the wind blows) was divided into eight sectors: North (N), North-East (NE), East (E), South-East (SE), South (S), South-West (SW), West (W) and North-West (NW). The kinetic energy $E_{n,i}$ crossing a vertical plane area was computed following Gerkema and Duran-Matute [2017], and can be written as follows:

$$E_{n,i} = \frac{1}{2}\rho A \Delta t \, W_{n,i}^3, \tag{1}$$

where ρ is the density of air (1.225 kg m^{-3}), A is the unit area of a vertical plane (1 m^2), Δt is the hourly interval in seconds and $W_{n,\,i}$ is the wind speed with a specific sectorial direction n and at hour i. It is worthwhile to notice that the eight sectors cannot be regarded as independent, since there are only two independent directions in a vectorial sense [Gerkema and Duran-Matute, 2017]. For sector n, the temporal mean energy is written as follows:

$$E_n = \frac{1}{M_a}\sum_i E_{n,i}, \tag{2}$$

where M_a is the total number of hours in the time series.

The sum of the wind energy across all the sectors is defined here as total wind energy (E):

$$E = \sum_n \sum_i E_{n,i}, \tag{3}$$

The total wind energy (E) is obtained from eq. (1) by computing the sum of the wind energy over all the sectors over the entire period of analysis. By contrast, the mean wind energy (E_n) is calculated from eq. (1) by computing the sum of the wind energy in sector n over the entire period of analysis and dividing by the total number of data points (i.e., number of hours).

3.3. Empirical orthogonal function (EOF) analysis

The 'empirical orthogonal function' analysis is applied to study the spatiotemporal changes in the residual volume transport across seven transects within the DWS (Fig. 1). This method was introduced by Lorenz [1956], and it enables the identification of spatial and temporal patterns in a dataset. The residual volume transport is computed from the instantaneous volume transport following two steps. First, we calculate the instantaneous transport through all the transects as follows:

$$Q = \int_A u dA, \tag{4}$$

where u is the velocity component normal to the transect of interest and

A is the transect cross-sectional area. Then, the residual volume flow is calculated employing a simple trapezoidal integration for every tidal period in 2005–2015. We use a definition of tidal period that is valid at a wide-basin scale, namely the time between two instants in which the instantaneous water volume in the system matches the long-term average volume during rising tides. The latter is the long-term average volume during the period 2005–2015 (Fig. 2a). This definition of tidal period has the advantage that the sum of the residual flow through the transects, rate of freshwater discharge, evaporation and precipitation equals zero [Duran-Matute and Gerkema, 2015]. A more classical definition of tidal period (e.g., the time between alternate slacks) cannot be applied at a basin scale due to differences in phase of the tide between different places (e.g., non-simultaneity of slacks), and hence, it has no basin-wide validity.

Once we have obtained the time series of the residual volume transport, we use the EOF analysis on the resulting time series. At first, we create a matrix (S) with the time series of the residual volume transport across the inlets and the shallow watersheds delimiting the system and each tidal basin. This matrix ('observation matrix') has n-rows and m-columns. Every column represents a time series at a specific inlet and watershed. Then, we remove the corresponding mean from each time series, and we compute the covariance matrix (C) of the anomalies (i.e., the difference between the original time series and the corresponding mean):

$$\mathrm{C} = F^T F, \tag{5}$$

where F^T is the transposed matrix of F, which stores the detrended time series. Finally, we solve the corresponding eigenvalue problem:

$$\mathrm{C} = \mathrm{V}\ \lambda\ V^T, \tag{6}$$

where λ is the eigenvalue matrix (positive definite) and V is the matrix with the corresponding eigenvectors (m-rows and m-columns). Each eigenvalue gives an indication of the fraction of the total variance captured by each eigenvector. This fraction (amount of variance related to each eigenvector) is calculated by dividing each eigenvalue by the trace of the eigenvalue matrix: λ_j/trace(λ).

The eigenvectors (indicated in the literature as 'empirical orthogonal functions' or 'EOFs') are ordered according to the size of the corresponding eigenvalue (e.g., EOF1 is the eigenvector associated with the largest eigenvalue). The covariance matrix in the new coordinate system, identified by the eigenvectors, is diagonal, and the variance in one direction is independent from the other directions. The observation matrix in the new space can be expressed as follows:

$$\mathrm{T} = \mathrm{F}\ \mathrm{V}. \tag{7}$$

Since the eigenvectors are ordered hierarchically, we can choose to employ only the first r EOFs to describe the dataset. In other words, we can build a matrix V_r (m x r) using the first r-columns of V and calculate a truncated matrix T_r (n x r):

$$\mathrm{T_r} = F\ \mathrm{V_r}. \tag{8}$$

This procedure reduces the dimensions of the observation matrix by projecting the data on the most important directions (i.e., principal components explaining most of the variance in the data). The columns in T_r represents the evolution of the eigenvectors in time, and they are known as 'expansion coefficients' (ECs).

3.4. Calculation of the volume and flushing time of fresh water

We calculated the volume of fresh water (V_k) from the tracer concentration resulting from the high-resolution numerical simulations. The freshwater volume inside the three tidal basins (each tidal basin was defined as in Ridderinkhof and Zimmerman [1990]) was computed as follows:

$$V_k = \int_V c_k dV, \tag{9}$$

where k (=1, 2) refers to the different sources of tracers, c_k is the tracer concentration and dV represents the volume of a pixel (i.e., grid cell) in the numerical domain. The flushing frequency of fresh water (Ω_k) is defined as

$$\Omega_k = \frac{\int_T R_k dt}{\int_T V_k dt}, \tag{10}$$

where R_k is the fresh water discharged in the system by each sluice (k = 1, 2).

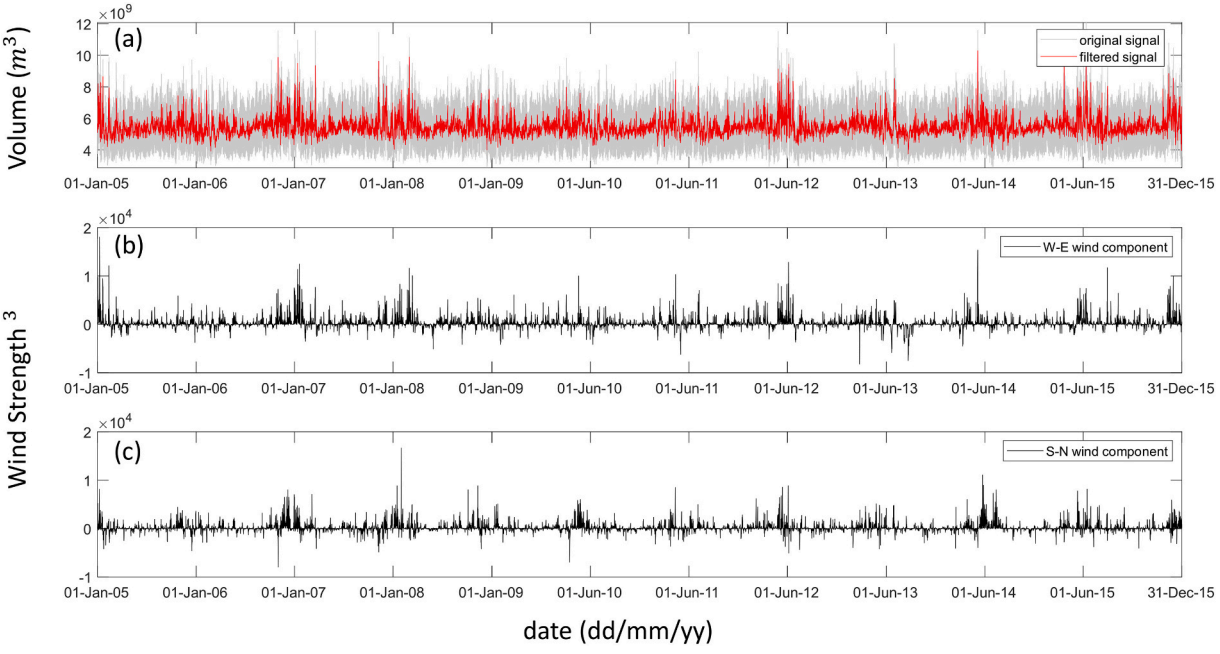

Fig. 2. (a) Time series and filtered signal of the water volume (m^3) within the DWS over the entire period of analysis. Cubic power of the vectorial wind components: (b) west-east component and (c) south-north component.

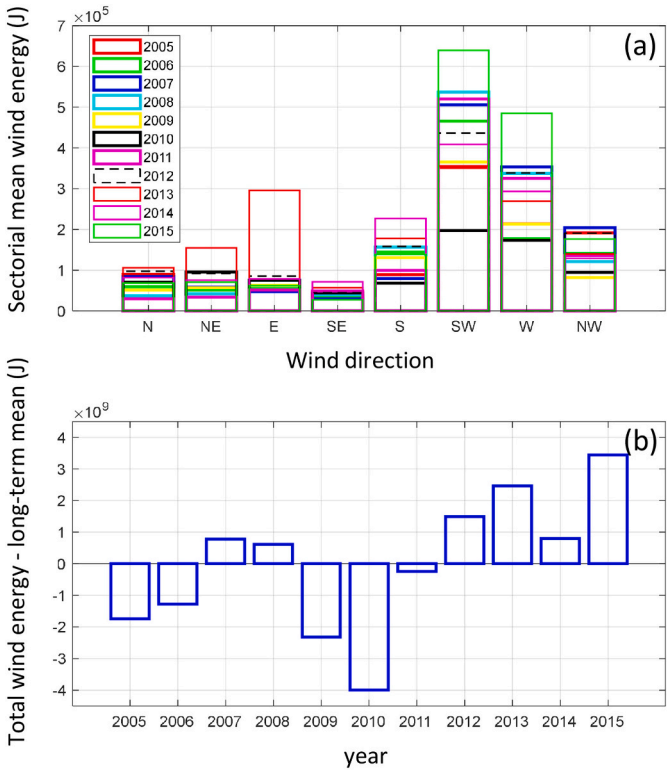

Fig. 3. Sectorial wind energy: (a) sectorial annual mean energy for all individual years and (b) differences between the total wind energy (i.e., sum of the wind energy across all the sectors for each year) and the mean total wind energy over the entire period of analysis.

3.5. Peak over threshold method

The 'peak over threshold' method (POT-method) is based on the analysis of the data exceeding a censoring critical value [D'Alpaos et al., 2013; Carniello et al., 2016]. According to the extreme value theory, threshold exceedances of stochastic signals are Poisson distributed [Cramér and Leadbetter, 1967; Leadbetter, 1991]. Here, we applied the POT-method to the flushing frequency time series to analyze statistically the occurrence of anomalous flushing values (clusters). The selection of the threshold is based on subjective considerations, but a common approach is to choose a fixed percentile (e.g., 95%, 99% or 99.5%) [e.g., Smith, 1990]. Moreover, a minimum time span between two consecutive anomalies (i.e., interarrival time) must be defined to have mutually independent clusters [e.g., Solari and Losada, 2012]. Further details of the method are described by D'Alpaos et al. [2013] and Carniello et al. [2016], who applied the POT-method for the analysis of the wave-induced bottom shear stresses and suspended sediment concentrations (SSC) in the Venice Lagoon.

4. Results

The instantaneous water volume within the DWS is shown in Fig. 2a (grey line). The time series exhibits a substantial temporal variability, mainly due to the wind forcing and tides. High frequency fluctuations (i.e., tidal oscillations) are removed from the original signal by applying a Lanczos low-pass filter, while the subtidal components induced by remote winds acting on the continental shelf adjacent to the DWS and local wind effects are retained (red line in Fig. 2a). We calculate the correlation coefficient between this 25 h-filtered signal and the cubic power of the vectorial components of the wind velocity (Fig. 2b, c). The cubic power of the east-west wind component produces a high correlation coefficient ($R = 0.64$) with the water volume. In contrast, there is no correlation with the cubic power of the south-north component ($R = 0.04$). The long-term mean of the filtered signal is 5.50×10^9 m^3 (the standard deviation is 5.45×10^8 m^3), and the skewness of the water-volume's distribution is positive ($s = 1.64$). This means that the time series experiences fluctuations around the long-term mean water volume much more in the positive direction (i.e., increase in water volume) than in the negative one (i.e., decrease in water volume). Fig. 2 shows that periods with large variability in the volume coincide with periods of strong winds (mostly during autumn and winter) and helps to visualize the large temporal variability induced by winds in the system's response (at short time scales). In addition, this time series (Fig. 2a) is used to compute the tidal periods for the entire period of analysis (as described in Subsection 3.3).

The wind energy (Fig. 3a) presents a substantial asymmetry in the distribution across the sectorial directions as well as a significant inter-annual variability (2010 is the year with the lowest wind energy, while 2015 is the year with the highest wind energy, see Fig. 3b). The south-westerly and westerly directions generally have the largest mean wind energy (Fig. 3a), but for 2010 the distribution across the sectors is much more even than for the other years. In the next subsections, special focus is devoted to understanding how the wind forcing affects the residual flow of water across different time scales. After investigating the tidally averaged transport of water, we explore temporal variations in freshwater retention over the period 2005–2015.

4.1. Residual circulation under calm conditions

Before analyzing the effect of the wind on the residual circulation, we study the residual flow at the inlets and shallow watersheds under calm conditions. First, we compute the instantaneous transport through all the transects with expression (4), and we calculate the tidally-averaged values from the hourly time series following the steps described in Subsection 3.3. Then, we remove from the statistics: (i) all the tidal periods characterized by a tidally averaged wind speed larger than 5 m/s, (ii) the three tidal periods which follow those with a tidally averaged velocity larger than 5 m/s. This step is crucial to remove those data characterized by calm conditions which are still influenced by past wind events; Oudijk [2021] found a typical memory of the system is at most three tidal periods. We take the residual volume flow to be positive if it

Table 1
Mean, median, standard deviation and skewness of the residual flow rate at the inlets and shallow watersheds under calm conditions (wind speed <5 m/s). The residual volume flow is considered positive if it corresponds to an inflow. For the watersheds 1 and 2, we consider these residual flows positive if they are directed towards the basins 2 and 3.

	Mean (m^3/s)	Median (m^3/s)	Standard deviation (m^3/s)	Skewness
Texel Inlet	−151.60	−163.83	$1.17 \cdot 10^3$	−0.03
Eierlandse Gat	−679.86	−610.69	452.77	0.64
Vlie Inlet	765.83	776.66	808.44	−0.04
Borndiep Inlet	−448.43	−438.76	645.41	−0.25
Watershed 1	248.69	200.77	$1.24 \cdot 10^3$	−0.10
Watershed 2	584.90	599.65	526.08	0.60
Watershed 3	−230.87	−243.87	139.13	−2.71

corresponds to an inflow, and negative if it corresponds to an outflow. Since the watersheds 1 and 2 are located within the system, we consider these residual flows positive if they are directed towards basins 2 and 3, respectively. The mean, median, standard deviation (which gives a measure of the tidally driven residual flow' temporal variations), and skewness of the residual flow under calm conditions are listed in Table 1, and discussed in Section 5.

4.2. Spatiotemporal variability in the residual circulation over the period 2005–2015

In this subsection, we compute the residual water volume flux over the entire period of analysis. Histograms of the residual flow rate across the four tidal inlets and the shallow watersheds are presented in Figs. 4 and 5 respectively. Table 2 shows the long-term mean, median, standard deviation and skewness for each distribution. It can be noted that the median is a better measure of the typical residual transport than the mean, since the former corresponds well with the peaks. The standard deviation expresses the variability of the residual flow associated with winds, tidal variations (e.g., spring-neap cycle), freshwater discharge and baroclinic effects. The standard deviation is largest at the Texel Inlet, followed by the watershed 1, the Vlie Inlet, the watershed 2 and the Borndiep Inlet. The Eirlandse Gat and the watershed 3 exhibit the lowest standard deviation, indicating that the residual flow through these transects is less sensitive to episodic events. All the histograms have an asymmetrical shape, and we notice that the long-term mean (and median) values have an opposite sign with respect to the skewness for the Eierlandse Gat and the Vlie Inlet. This means that the absolute values of the extremes are greater for the outflow rather than for the inflow in these tidal inlets. To highlight the year-to-year changes in the residual transport, we plot the median and standard deviation for each year in Fig. 6. All the transects show the lowest standard deviation in 2010 (the year with the lowest wind energy), while the highest standard deviation is registered for the year 2008 (which presents with years 2007 and 2015 the largest energy associated with southwesterly, westerly and northwesterly winds). The inter-annual variability of the standard deviation exhibits a similar pattern for each transect from 2008 onward, whereas we cannot detect a general trend for the first three

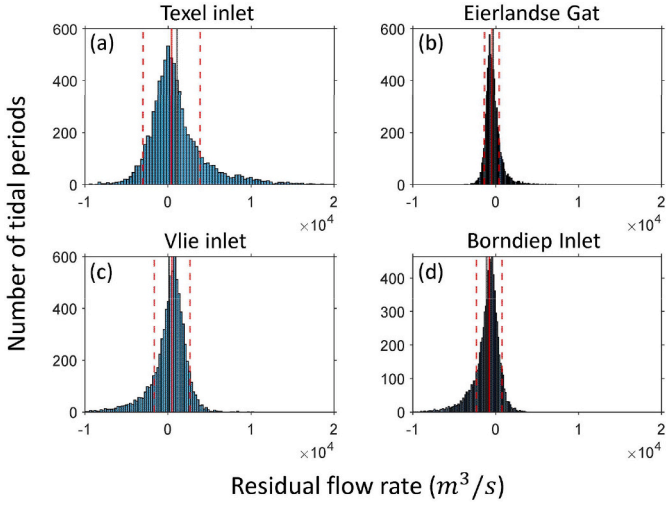

Fig. 4. Histograms of the residual flow rate through the inlets (red transects in Fig. 1). The solid red line represents the median value, while the dashed lines represent the median value plus/minus one standard deviation. The black line represents the mean value. The residual volume flow is considered positive if it corresponds to an inflow. For the watersheds 1 and 2, we consider these residual flows positive if they are directed towards the tidal basins 2 and 3. (For interpretation of the references to colour in this figure legend, the reader is referred to the web version of this article.)

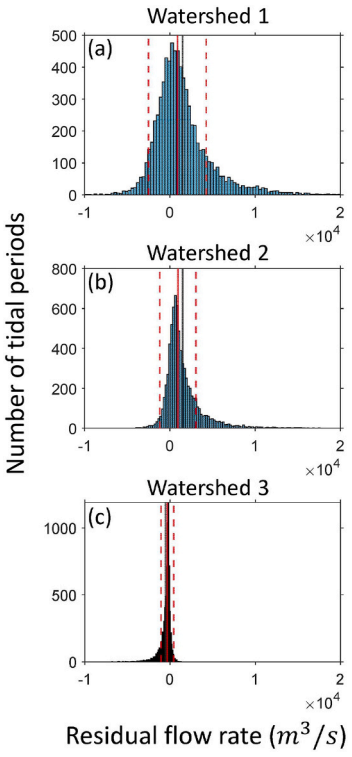

Fig. 5. Histograms of the residual flow rate through the shallow watersheds (red transects in Fig. 1). The solid red line represents the median value, while the dashed lines represent the median value plus/minus one standard deviation. The black line represents the mean value. The residual volume flow is considered positive if it corresponds to an inflow. For the watersheds 1 and 2, we consider these residual flows positive if they are directed towards the tidal basins 2 and 3. (For interpretation of the references to colour in this figure legend, the reader is referred to the web version of this article.)

years of analysis.

To identify what external forces contribute to the variability in the residual transport, we removed the corresponding mean from each time series, and we applied the EOF decomposition. It is worthwhile noticing that the signs of the residual flow for the watersheds 1 and 2 do not impact the outcome of our analysis. A different choice would flip only the sign of the eigenvectors' values for these two transects. Our results show that the first three eigenvalues explain most of the variability in the dataset. Specifically, their contribution to the total variance is: 85.7% for the first mode, 8.4% for the second mode and 5.3% for the third mode. To each eigenvalue, the EOF analysis identifies an eigenvector. The eigenvectors are depicted in Fig. 7, and they are ordered hierarchically according to the eigenvalues' magnitude. The first three modes suggest that the Texel inlet (inlet A) and the Eierlandse Gat (inlet B) have an opposite behavior with respect to the Vlie Inlet (inlet C) and the Borndiep Inlet (inlet D). Hence, the fluctuations around the mean have opposite signs for the Texel inlet and the Vlie Inlet, and for the Eierlandse Gat and the Borndiep Inlet. It is simple to demonstrate that multiplying each eigenvector in the Eierlandse Gat (inlet B, Fig. 7) and in the Borndiep inlet (inlet D, Fig. 7) by the corresponding expansion coefficients (Fig. 8), the resulting signals (i.e., three time series for each transect) have opposite oscillations. The sum of these three signals in each transect represents the difference between the actual residual transport and its temporal mean.

We present the expansion coefficients (ECs) and their yearly means in Fig. 8, and the histograms associated with each EC in Fig. 9. Table 3 shows the median, standard deviation and skewness for each of them. The distribution of the first two expansion coefficients is strongly asymmetric (skewness: −1.78 and −1.89). By contrast, the distribution

Table 2
Mean, median, standard deviation and skewness of the residual flow rate at the inlets and shallow watersheds calculated for the entire period of analysis. The residual volume flow is considered positive if it corresponds to an inflow. For the watersheds 1 and 2, we consider these residual flows positive if they are directed towards the basins 2 and 3.

	Mean (m^3/s)	Median (m^3/s)	Standard deviation (m^3/s)	Skewness
Texel Inlet	$1.06 \cdot 10^3$	410.60	$3.43 \cdot 10^3$	1.55
Eierlandse Gat	−350.80	−492.60	905.50	1.77
Vlie Inlet	148.50	494.30	$2.13 \cdot 10^3$	−1.40
Borndiep Inlet	$-1.06 \cdot 10^3$	−775.70	$1.53 \cdot 10^3$	−1.46
Watershed 1	$1.50 \cdot 10^3$	881.09	$3.38 \cdot 10^3$	1.58
Watershed 2	$1.51 \cdot 10^3$	947.90	$2.12 \cdot 10^3$	2.27
Watershed 3	−522.10	−322.50	732.09	−3.28

of the third expansion coefficient presents a low skewness (−0.36), indicating that the oscillations are almost symmetric. It was found that the wind and the freshwater discharge are the best predictor variables to explain all the modes. Figs. 10 and 11 show the three expansion coefficients, the cubic power of the vectorial components of the wind velocity, and the total freshwater discharge. For illustrative purposes, we plotted the first two expansion coefficients multiplied by −1 and for only the first 1000 tidal cycles (Fig. 10). The first two expansion coefficients present a good correlation with the cubic power of the S—N vectorial wind component ($|R|$=0.62), and the cubic power of the W-E vectorial wind component ($|R|$=0.63). Finally, the third expansion coefficient exhibits a moderate correlation ($|R|$=0.57) with the total freshwater discharge (Fig. 11). The signals depicted in Fig. 11 (biweekly time series) are filtered with a cut-off period of 30 tidal periods, because the effects of the freshwater discharge are relevant at time scales longer than a tidal period.

4.3. *Long-term residual transport over the period 2005–2015 (without extreme events)*

We calculate the long-term residual flow at the inlets and shallow watersheds over the entire period of analysis by removing from the statistics those tidal periods characterized by strong winds. Tidally averaged wind speeds present a median of 6.21 m/s (mean of 6.61 m/s),

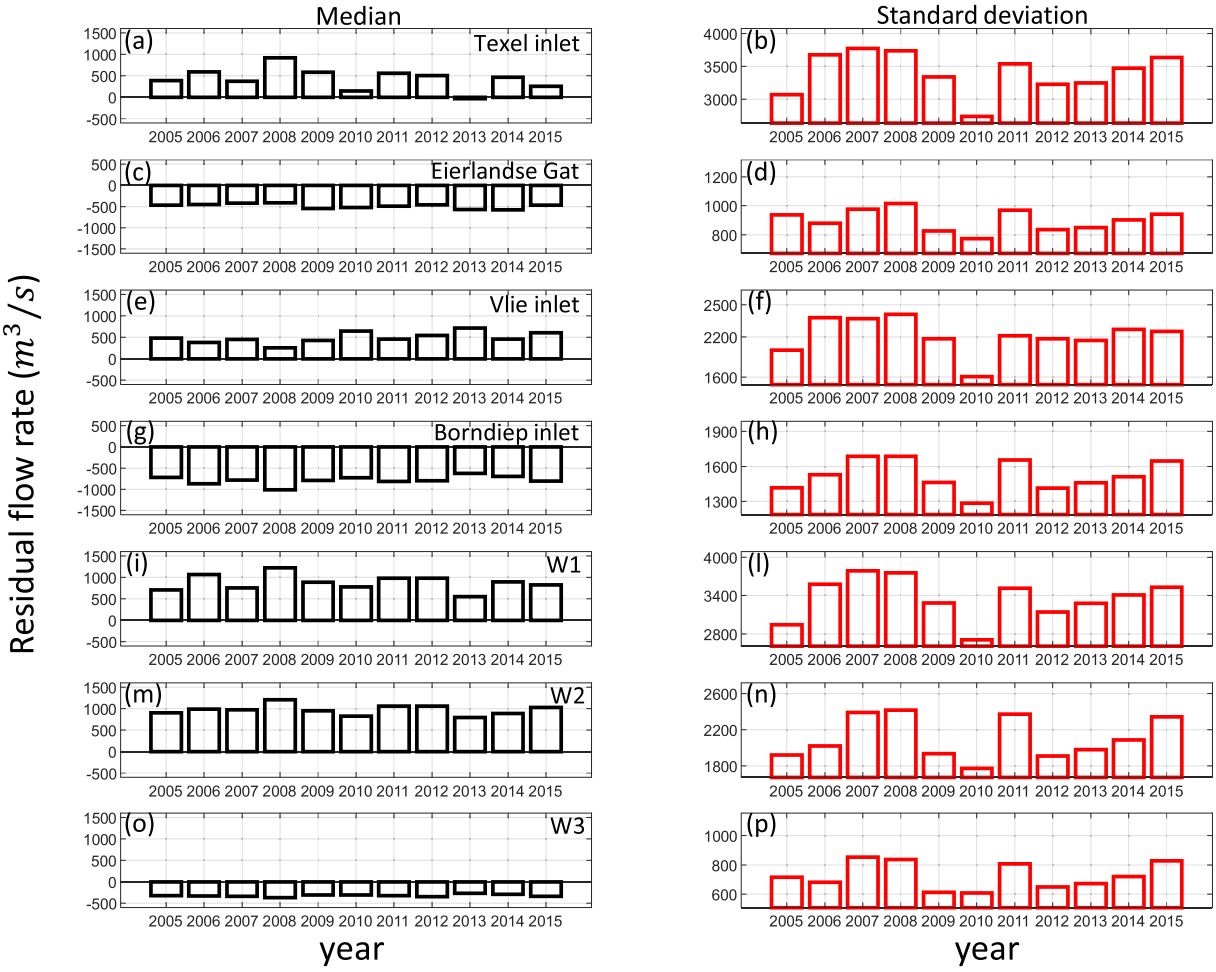

Fig. 6. Median (a, c, e, g, i, m, o) and standard deviation (b, d, f, h, l, n, p) of the residual volume flow in each transect for each year. The residual volume flow is considered positive if it corresponds to an inflow. For the watersheds 1 and 2, we consider these residual flows positive if they are directed towards the tidal basins 2 and 3.

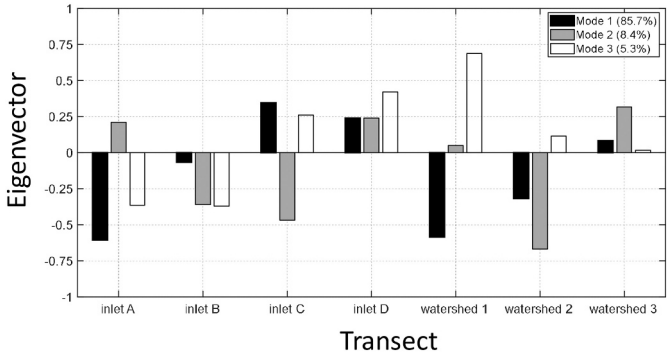

Fig. 7. EOF analysis of the residual transport across the inlets and the shallow watersheds delimiting each tidal basin (red transects in Fig. 1). Eigenvectors for the first three modes. (For interpretation of the references to colour in this figure legend, the reader is referred to the web version of this article.)

and a standard deviation of 3.08 m/s. We eliminate from the statistics those tidal periods with a tidally averaged wind speed larger than 12 m/s (95th percentiles) and the three tidal periods following a tidal period characterized by extreme conditions (we remove 15% of the data). The long-term mean, median, standard deviation, and skewness of the residual flow under these conditions are reported in Table 4. By comparing the residual flow statistics with and without extreme events (Tables 2 and 4), we notice that extreme winds affect the long-term residual flow across the transects. In particular, the Texel inlet and the watershed W1 exhibit the largest changes in the long-term residual transport, while the Eierlandse Gat and the watershed W3 exhibit the smallest changes. The implications of this finding are discussed in Section 5.

4.4. Temporal variability in the flushing time of fresh water over the period 2005–2015

We used two different tracers to tag the freshwater dispersal in the system. First, the tracer concentrations resulted from the numerical

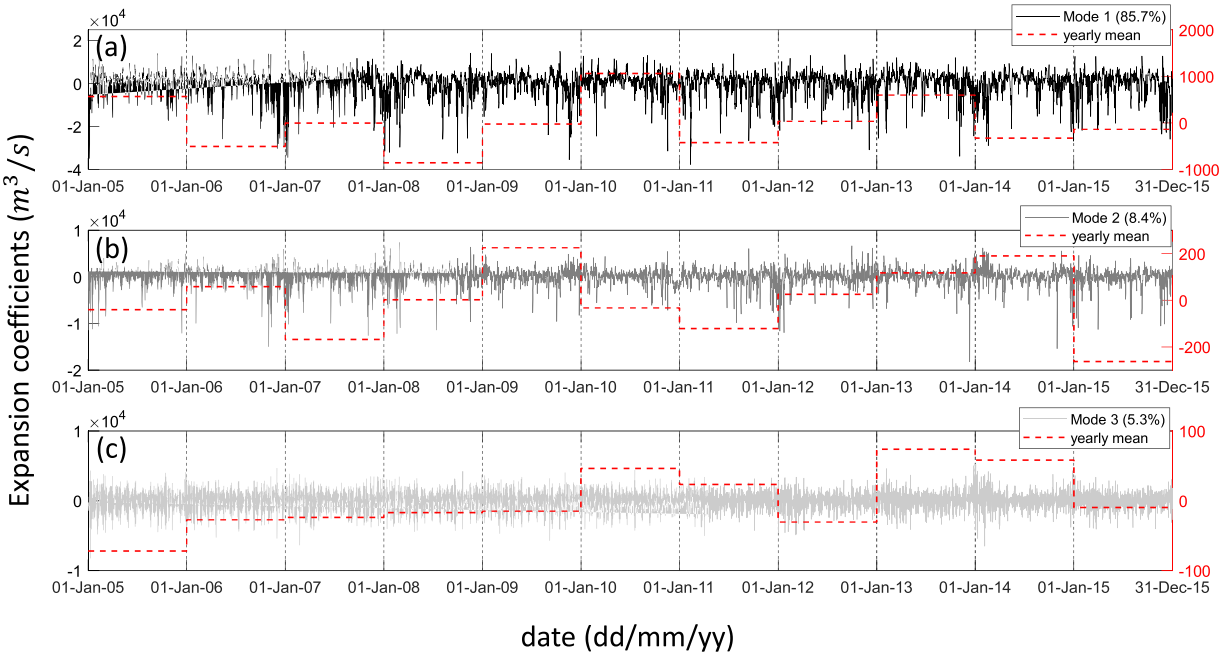

Fig. 8. EOF analysis of the residual transport across the inlets and the shallow watersheds delimiting each tidal basin (red transects in Fig. 1). Expansion coefficients for the first three modes (black lines) and their yearly mean values (red dashed lines). (For interpretation of the references to colour in this figure legend, the reader is referred to the web version of this article.)

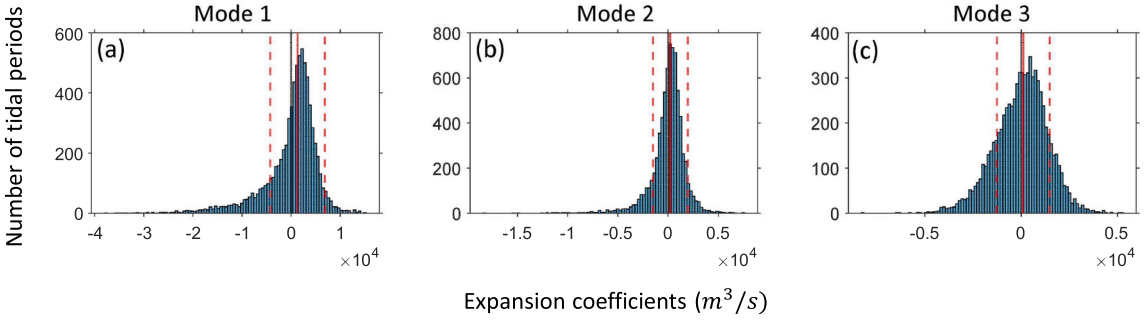

Fig. 9. Histograms of the expansion coefficients. The solid red line represents the median value, and the dashed lines represent the median value plus/minus one standard deviation. (For interpretation of the references to colour in this figure legend, the reader is referred to the web version of this article.)

Table 3
Median, standard deviation and skewness of the expansion coefficients.

	Median (m^3/s)	Standard deviation (m^3/s)	Skewness
EC-1	$1.29 \cdot 10^3$	$5.56 \cdot 10^3$	−1.78
EC-2	222.80	$1.74 \cdot 10^3$	−1.89
EC-3	105.40	$1.38 \cdot 10^3$	−0.36

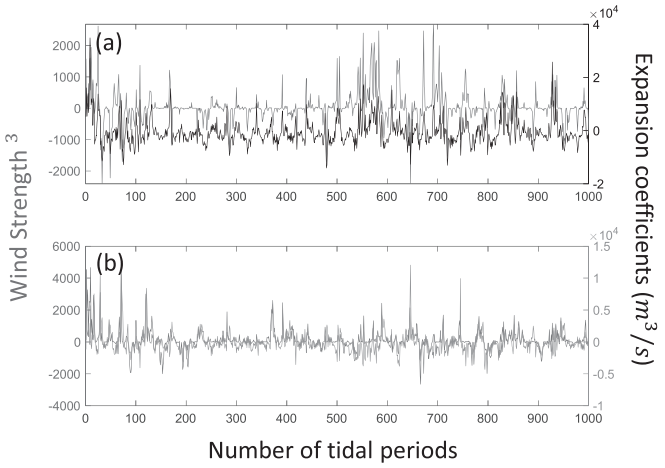

Fig. 10. Expansion coefficients and predictor variables (within-day time scale): (a) cubic power of the S—N vectorial wind component and first expansion coefficient multiplied by −1, and (b) cubic power of the W-E vectorial wind component and second expansion coefficient multiplied by −1.

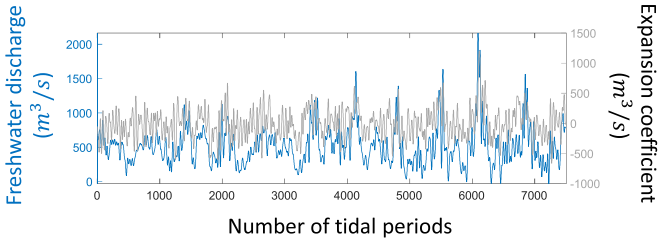

Fig. 11. Expansion coefficients and predictor variables (biweekly time scale): fresh water discharged into the system by the two sluices and third expansion coefficient.

modeling simulations were collected for each pixel (i.e., grid cell) of the numerical domain over the entire period of analysis. Then, we mapped the spatial distributions of the long-term mean and standard deviation from the hourly values (Fig. S1). Fig. S1 shows that the Den Oever tracer typically resides within the southern part of the system, whereas the Kornwerderzand tracer is distributed over a wider area. In general, the deep channels have the lowest tracer concentrations, while the tidal flats and the areas next to the sluices exhibit the largest mean values and standard deviations. High tracer concentrations over the tidal flats are not equivalent to large freshwater volumes. Thus, we calculated the freshwater volume for each numerical cell. Fig. 12 depicts the volume of fresh water (mean and standard deviation) within the DWS from Den Oever (Fig. 12a, c) and Kornwerderzand (Fig. 12b, d). As expected, the deep channels connecting the back-barrier basins to the North Sea carry most of the freshwater volume. In particular, the fresh water coming from Den Oever is transported by the channels leading to Texel Inlet, while the fresh water discharged by Kornwerderzand is distributed more uniformly among all the inlets. From the instantaneous freshwater volume calculated for each pixel, we compute the total freshwater volume stored within the three basins. Then, the flushing frequency for each tracer is obtained by using expression (10). Once the time series is obtained, the long-term mean, median, standard deviation and skewness are computed (Table 5). These values fall well within the range of those available in the literature [e.g., Zimmerman, 1976; Duran-Matute et al., 2014]. The flushing frequency's time series for each tracer is presented in Fig. 13. Histograms of the flushing frequency of fresh water are presented in Fig. S2. We notice that the median is a better measure of the typical flushing frequency than the mean. In addition, the ratio of the standard deviation to the median indicates a larger variability for the flushing frequency of fresh water discharged at Kornwerderzand.

The flushing frequency's time series for each tracer shows marked temporal variations. We perform a statistical characterization of the extreme flushing events' occurrence based on the peak over threshold method (POT-method, Subsection 3.5) to compute the typical interarrival time between two events characterized by extreme flushing values. We choose the 99th percentiles (red lines in Fig. 13) of the modeled time series as a critical value. The flushing frequencies corresponding to the 99th percentiles are: 0.35 day^{-1} and 0.52 day^{-1} for Den Oever and Kornwerdenzand respectively. First, we construct the POT data series of independent observations by taking the maximum value of each cluster. Then, the minimum interarrival time is chosen such that the lag one autocorrelation coefficient of the POT series is close to zero [e.g., Solari and Losada, 2012]. The minimum interarrival time satisfying the above condition is four tidal periods (which represents a measure of the system's memory). Table 5 contains the mean interarrival time of extreme flushing episodes of fresh water for Den Oever and Kornwerdenzand.

Table 4
Mean, median, standard deviation and skewness of the residual flow rate at the inlets and shallow watersheds calculated for the entire period of analysis (excluding extreme events). The residual volume flow is considered positive if it corresponds to an inflow. For the watersheds 1 and 2, we consider these residual flows positive if they are directed towards the basins 2 and 3.

	Mean (m^3/s)	Median (m^3/s)	Standard deviation (m^3/s)	Skewness
Texel Inlet	441.54	198.39	$2.44 \cdot 10^3$	0.74
Eierlandse Gat	−494.08	−564.14	669.73	0.54
Vlie Inlet	461.32	622.32	$1.60 \cdot 10^3$	−0.79
Borndiep Inlet	−747.56	−661.34	$1.08 \cdot 10^3$	−0.42
Watershed 1	870.47	622.10	$2.40 \cdot 10^3$	0.77
Watershed 2	$1.05 \cdot 10^3$	807.44	$1.34 \cdot 10^3$	1.07
Watershed 3	−379.19	−281.48	437.44	−1.6

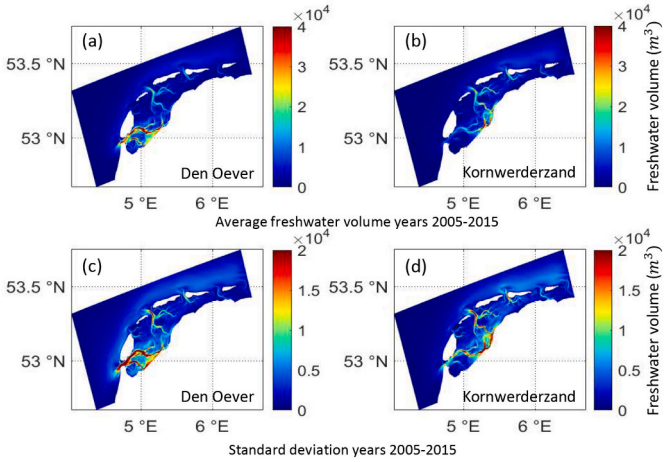

Fig. 12. These maps represent the long-term mean freshwater distribution (a, b) and standard deviation (c, d) in the DWS for Den Oever and Kornwerderzand. The period of analysis is 2005–2015.

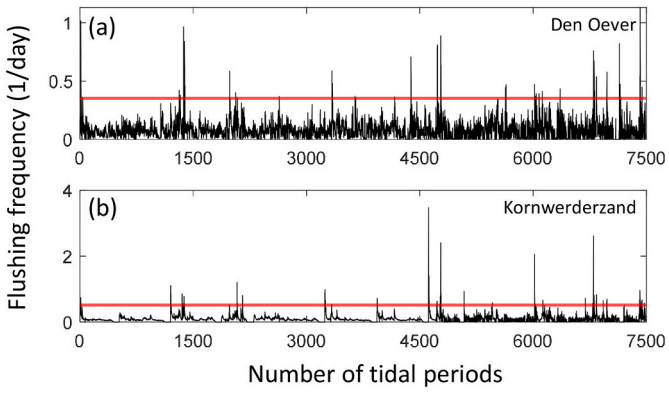

Fig. 13. Flushing frequency of fresh water: (a) Den Oever and (b) Kornwerderzand. The red lines represent the 99nd percentiles. (For interpretation of the references to colour in this figure legend, the reader is referred to the web version of this article.)

5. Discussion

The impact of the wind forcing on the residual circulation and freshwater flushing within an interconnected system of intertidal basins has been evaluated for the Dutch Wadden Sea. The system has two major agents in water movements: the tides and the wind. While the former is highly predictable, the latter is episodic in nature. The wind climate varies even strongly from year to year. The analyses are based on high-resolution numerical modeling simulations spanning the years 2005–2015. The length of the simulations allowed us to: (i) evaluate the effect of the wind under a wide range of circumstances, (ii) identify the interannual variability in the residual transport, (iii) quantify the long-term typical residual flow, and (iv) study the flushing frequency of fresh water across different time scales.

5.1. Tidally-driven and wind-driven residual water volume flow

In the previous sections, we computed the tidally-driven residual volume flow by using only those tidal periods characterized by wind speeds smaller than 5 m/s (Table 1). Our results show that the wind opposes the tidally-driven flow in three inlets (i.e., Texel inlet, Eierlandse Gat, Vlie inlet), and reverses the direction of the residual transport computed under calm conditions for the Texel inlet. In particular, the tidally averaged volume flow in the Texel inlet is negative (i.e., outflow) under calm conditions, and positive (i.e., inflow) when winds and storms take place (Tables 2–4). This finding reveals that winds and extreme events not only alter the residual flow at short time scales, but they leave, despite their episodic nature, a mark on its long-term mean (and median) values. By contrast, the wind strengthens the tidally-driven residual flow through the three watersheds and the Borndiep inlet. Episodic events enhance the exchange between the intertidal basins, and facilitate the water transport across the shallow watersheds by increasing water levels (i.e., wind surges). Specifically, the water exchange between the intertidal basins will be enhanced (or reduced) by those wind directions inducing set-up (or set-down) of water level.

The effect of the wind on the residual circulation presents a strong spatial variability. The ratio between the standard deviation and the median of the residual transport shows that the Texel inlet exhibits the highest sensitivity to the wind, whereas the Eierlandse Gat and the W3 show very little variability. In addition, the transects present preferential wind directions which enhance the tidally averaged flow. The Eierlandse Gat (inlet B, Fig. 1) shows a greater residual transport for winds in the east-west direction, since the product between the second eigenvector (computed in this inlet) and the second expansion coefficient is larger compared to the product between the first eigenvector and the first expansion coefficient (Figs. 7, 8). In contrast, the other tidal inlets are more sensitive to winds in the south-north direction. This finding further corroborates previous numerical modeling results [Duran-Matute et al., 2016].

5.2. Interaction between the intertidal basins and consequences for the residual flow

As discussed in Subsection 5.1, the long-term median residual flow through the Texel inlet is positive (i.e., inflow into the DWS). The direction of the residual transport in this inlet influences the circulation not only in basin 1 but also in the remainder of the DWS, since the intertidal basins are interconnected. The total (cumulative) water volume entering via the Texel inlet over the period 2005–2015 must leave the system through the other tidal inlets and/or the easternmost shallow watershed. To explain how the interaction between the intertidal basins affects the long-term residual flow, we focus on the tidal basin 2. The latter receives a certain amount of water from basin 1 via the shallow watershed W1, which is the sum of the total fresh water discharged by the two sluices and the cumulative water volume coming from the Texel inlet. The total water volume calculated along the transects delimiting basin 2 is zero (for the conservation of mass), thus the cumulative water volume computed across the watershed W1 must be balanced by the sum of the water volume through the other three transects (i.e., Eierlandse Gat, Vlie inlet, watershed W2). This reasoning explains how the long-term residual flow in basin 2 is affected by the inflow occurring in the Texel inlet. The same argument is valid also for basin 3. In addition, we notice that the residual transport at the shallow watersheds W1 and W2 dominates the circulation in the intertidal basins 1 and 2, since the tidally averaged flow in these transects is much larger than at the inlets. In contrast, the residual transport through the Borndiep inlet is larger than the residual flow across the watershed W3 (basin 3).

Table 5
Mean flushing frequency, median flushing frequency, standard deviation, skewness and mean interarrival time of the over-threshold events.

	Mean (1/days)	Median (1/days)	Standard deviation (1/days)	Skewness	Mean interarrival time, over-threshold events (tidal periods)
Den Oever	0.080	0.067	0.078	3.209	223
Kornwerdenzand	0.096	0.074	0.125	9.954	231

5.3. Wind forcing: Consequences for the yearly residual transport

The relationship between wind and residual transport comes into play on short timescales (one tidal period), but this relationship is also clear at longer time scales. The variability induced by the wind is reflected by the standard deviation of the residual flow across the inlets and the shallow watersheds, which is one order of magnitude larger than the long-term median value in certain transects (Table 2). Annual median residual transports vary strongly from year to year (with the extreme values occurring in 2008 and 2013), and this variability can be related to the wind conditions (Figs. 3 and 6). For instance, the median residual flow exhibits a marked inter-annual variability for the Texel Inlet, and an inversion in the direction of the tidally averaged transport is found in 2013. Indeed, this year is characterized by the largest wind energy for the NE and E sectorial wind directions (Fig. 3a). Moreover, the minimum standard deviation (the lowest variability) in each transect coincides with the year characterized by the lowest wind energy (i.e., 2010). This means that the inter-annual variability in the residual transport can mainly be ascribed to the prevailing wind conditions in each particular year, since we identified a clear correspondence between the annual mean wind energy and the residual flow's yearly characteristics.

Our results reveal that the wind forcing controls the residual circulation in the Dutch Wadden Sea at short (i.e., one tidal cycle) and long (i.e., years) time scales. In addition, episodes characterized by high-wind speeds, albeit rare, are strong and their aggregate effect impacts on the typical residual flow (i.e., long-term median). Since winds and storms make the system's response strongly deviating from its long-term typical state across different time scales (i.e., the DWS behaves like an event-driven system), the dynamics cannot be seen as a statistically steady (i.e., as if the cyclical tides were the dominant agent in water movements). Therefore, this episodic character in the hydrodynamics must be taken into account when analyzing the long-term exchange of sediments, nutrients, fresh water and pollutants between the system and the North Sea. These findings could be extended to other coastal systems exhibiting the same event-driven nature of the DWS (e.g., Mediterranean lagoons, shallow coastal bays along the East Coast of United States) and be particularly important to predict their fate under climate change. Numerous studies highlight the importance of the wind forcing and storms on the sediment budget [e.g., Nowacki and Ganju, 2018; Pannozzo et al., 2021], and erosional processes [e.g., Valentine and Mariotti, 2019; Cortese and Fagherazzi, 2022] in shallow coastal bays, but the cumulative impact of short-duration events on the inter-annual variability and long-term response of these systems has been neglected due to the lack of data spanning several years/decades. The approach used here for understanding the role of the wind in the DWS' dynamics could be applied to other wind-driven coastal environments around the world. More specifically, these systems may respond less or more strongly to the wind forcing depending on their mean water depth and orientation with respect to the dominant wind (e.g., the DWS is aligned with the dominant southwesterly wind).

5.4. Flushing frequency of fresh water

The flushing frequency of fresh water in a multiple-inlet coastal system depends on: (i) the amount of fresh water discharged into the back-barrier basins, and (ii) the freshwater volume retained in each tidal cycle. The latter is ultimately controlled by the residual transport of fresh water at the transects delimiting the system [Duran-Matute et al., 2014]. Therefore, temporal changes in the flushing can be related to the variability in the freshwater discharge and wind forcing. The flushing frequency's time series for each tracer reveals abrupt temporal variations in the DWS, bearing out the event-driven nature of the system (Fig. 13). Duran-Matute et al. [2014] linked the occurrence of events characterized by extreme flushing values to the wind climate for the period 2009–2010. In the present study, we quantify the interarrival time of these episodes. Moreover, median values exhibit a marked inter-annual variability. For instance, the median flushing frequency for each tracer in 2010 (the year with the lowest wind energy, Fig. 3b) is 0.075 day^{-1} and 0.066 day^{-1} for Den Oever and Kornwerdenzand respectively. By contrast, the median flushing frequencies are 0.064 day^{-1} and 0.077 day^{-1} in 2015 (the year with the largest wind energy, Fig. 3b). This is plausibly related to the fact that south-westerly and westerly winds in 2010 (Fig. 3a) are not strong enough to push the fresh water into the eastern part of the DWS. Thus, the fresh water released by Den Oever leaves the system mainly via Texel inlet, resulting in a median flushing frequency greater than its median value computed over the entire period of analysis (i.e., 0.067 day^{-1}). This finding further confirms that the wind plays a crucial role in water movements within the system as suggested by previous researches [e.g., Donatelli et al., 2022]. In particular, Donatelli et al. [2022] showed the importance of the wind forcing on the freshwater dispersal in the DWS by applying advanced statistical methods to study the occurrence of clusters (i.e., estuarine regions characterized by strong deviations from the expected salinity values in a statistical sense) in the salinity field at event-scale. More specifically, they related the presence of anomalous salinity values in various sub-regions of the system to episodic events characterized by extreme conditions in the southwesterly wind and freshwater discharge.

6. Conclusions

Event-driven intertidal basins are highly dynamic coastal environments, where the wind forcing plays a fundamental role in their dynamics. Since their long-term (i.e., yearly) statistics are highly variable due to the occurrence of incidental events (e.g., storms), the hydrodynamics in these systems cannot be studied as statistically steady (i.e., governed mainly by the repetitive tidal cycles). Given the episodic character of the variability and the paramount effect of sporadic events at time scale of hours to days on annual median values, long-term numerical modeling simulations are needed to study these coastal environments in a meaningful statistical way.

In this paper, we use high-resolution numerical modeling simulations spanning several years (2005–2015) to analyze the temporal variability in residual circulation and freshwater retention in the Wadden Sea. We focus on the Dutch part of the Wadden Sea between the Texel inlet and the Groninger Wad. The DWS exhibits a complex dynamics and strong spatial heterogeneity in terms of tidal prisms, freshwater discharge, and basin size and depth. From an ecological point of view, too, the intertidal basin shows both inter-annual variability and spatial diversity [e.g., Compton et al., 2013; Schwichtenberg et al., 2017]. Our results highlight that the wind forcing significantly alters the system's response making it strongly deviate from its long-term typical state (i.e., it behaves like an event-driven system). In particular, we show that the behavior of the DWS presents strong deviations from its long-term mean (or median) conditions across different time scales, with a potential impact on the exchange of water, larvae, nutrients and sediments between the tidal basins and the North Sea. More specifically, the response of the system in terms of residual transport and flushing frequency of fresh water can deviate largely from the long-term mean (or median) value. For instance, the time series of the freshwater flushing frequency presents abrupt temporal variations revealing the event-driven nature of the DWS. Our findings highlight that the wind forcing creates a marked variability at year-to-year time scale, and we found that extreme events, albeit rare, affect the long-term typical state of the system. This paper underlines the fundamental role of the wind in water movements within event-driven systems.

Declaration of Competing Interest

The authors declare that they have no known competing financial interests or personal relationships that could have appeared to influence the work reported in this paper.

Data availability

Data will be made available on request.

Acknowledgements

We thank the four anonymous Reviewers for their comments. This study was supported by the NWO/ENW project: 'The Dutch Wadden Sea as an event-driven system: long-term consequences for exchange (LOCO-EX)'. The work was supported by the North-German Supercomputing Alliance (HLRN). Data are available online (https://zenodo.org/search?page=1&size=20&q=carmine%20donatelli).

Appendix A. Supplementary data

Supplementary data to this article can be found online at https://doi.org/10.1016/j.seares.2022.102242.

References

Blake, R.A., 1991. The dependence of wind stress on wave height and wind speed. J. Geophys.Res. 96, 20531–20545.
Bolin, B., Rodhe, H., 1973. A note on the concepts of age distribution and transit time in natural reservoirs. Tellus 25, 58–62.
Burchard, H., Bolding, K., 2002. GETM: a general estuarine transport model, Scientific documentation. In: Tech. Rep. EUR 20253 EN. Eur. Comm, Ispra, Italy.
Burkholder, J.M., Tomasko, D.A., Touchette, B.W., 2007. Seagrasses and eutrophication. J. Exp. Mar. Biol. Ecol. 350, 46–72.
Carniello, L., D'Alpaos, A., Botter, G., Rinaldo, A., 2016. Statistical characterization of spatio temporal sediment dynamics in the Venice lagoon. J. Geophys. Res. Earth Surf. 121, 1049–1064. https://doi.org/10.1002/2015JF003793.
Compton, T.J., Holthuijsen, S., Koolhaas, A., Dekinga, A., Ten Horn, J., Smith, J., Galama, Y., Brugge, M., Van Der Wal, D., Van Der Meer, J., Van Der Veer, H.W., Piersma, T., 2013. Distinctly variable mudscapes: distribution gradients of intertidal macrofauna across the Dutch Wadden Sea. J. Sea Res. 82, 103–116.
Cortese, L., Fagherazzi, S., 2022. Fetch and distance from the bay control accretion and erosion patterns in Terrebonne marshes (Louisiana, USA). Earth Surf. Process. Landf. 47 (6), 1455–1465.
Cramér, H., Leadbetter, M.R., 1967. Stationary and Related Stochastic Processes. John Wiley, New York, p. 348.
D'Alpaos, A., Carniello, L., Rinaldo, A., 2013. Statistical mechanics of wind wave-induced erosion in shallow tidal basins: inferences from the Venice lagoon. Geophys. Res. Lett. 40, 3402–3407. https://doi.org/10.1002/grl.50666.
Donatelli, C., Ganju, N.K., Kalra, T.S., Fagherazzi, S., Leonardi, N., 2019. Changes in hydrodynamics and wave energy as a result of seagrass decline along the shoreline of a microtidal back-barrier estuary. Adv. Water Resour. 128, 183–192.
Donatelli, C., Duran Matute, M., Gräwe, U., Gerkema, T., 2022. Statistical detection of spatio-temporal patterns in the salinity field within an inter-tidal basin. Estuar. Coasts. https://doi.org/10.1007/s12237-022-01089-3.
Duran-Matute, M., Gerkema, T., 2015. Calculating residual flows through a multiple-inlet system: the conundrum of the tidal period. Ocean Dyn. 65 (11), 1461–1475. https://doi.org/10.1007/s10236-015-0875-1.
Duran-Matute, M., Gerkema, T., de Boer, G.J., Nauw, J.J., Gräwe, U., 2014. Residual circulation and freshwater transport in the Dutch Wadden Sea: a numerical modelling study. Ocean Sci. 10 (4), 611–632. https://doi.org/10.5194/os-10-611-2014.
Duran-Matute, M., Gerkema, T., Sassi, M.G., 2016. Quantifying the residual volume transport through a multiple-inlet system in response to wind forcing: the case of the western Dutch Wadden Sea. J. Geophys. Res. Oceans 121, 8888–8903. https://doi.org/10.1002/2016JC011807.
Frank, C.W., Wahl, S., Keller, J.D., Pospichal, B., Hense, A., Crewell, S., 2018. A novel data set for solar energy applications based on high resolution reanalysis. Sol. Energy 164, 12–24.
Gerkema, T., 2019. An Introduction to Tides. Cambridge University Press, Cambridge. https://doi.org/10.1017/9781316998793.
Gerkema, T., Duran-Matute, M., 2017. Interannual variability of mean sea level and its sensitivity to wind climate in an inter-tidal basin. Earth Syst. Dynam. 8 (4), 1223–1235. https://doi.org/10.5194/esd-8-1223-2017.
Gräwe, U., Floser, G., Gerkema, T., Duran-Matute, M., Badewien, T.H., Schulz, E., Burchard, H., 2016. A numerical model for the entire Wadden Sea: skill assessment and analysis of hydrodynamics. J. Geophys. Res. Oceans 121, 5231–5251. https://doi.org/10.1002/2016JC011655.
Jiang, L., Soetaert, K., Gerkema, T., 2019. Decomposing the intra-annual variability of flushing characteristics in a tidal bay along the North Sea. J. Sea Res. 155, 101821.
Jung, A.S., Brinkman, A.G., Folmer, E.O., Herman, P.M.J., van der Veer, H.W., Philippart, C.J.M., 2017. Long-term trends in nutrient budgets of the western Dutch Wadden Sea (1976–2012). J. Sea Res. 127, 82–94.
Kara, A.B., Hurlburt, H.E., Wallcraft, A.J., 2005. Stability-dependent exchange coefficients for air-sea fluxes. J. Atmos. Oceanic Technol. 22, 1080–1094.
Kemp, W.M., Boynton, W.R., Adolf, J.E., Boesch, D.F., Boicourt, W.C., Brush, G., Cornwell, J.C., Fisher, T.R., Glibert, P.M., Hagy, J.D., Harding, L.W., Houde, E.D., Kimmel, D.G., Miller, W.D., Newell, R.I.E., Roman, M.R., Smith, E.M., Stevenson, J. C., 2005. Eutrophication in Chesapeake Bay: historical trends and ecological interactions. Mar. Ecol. Prog. Ser. 303, 1–29.
Kennish, M.J., 2001. State of the estuary and watershed: an overview. J. Coast. Res. 243 (32), 273. Special Issue.
Kondo, J., 1975. Air–sea bulk transfer coefficients in diabatic conditions. Bound.-Layer Meteorol. 9, 91–112. https://doi.org/10.1007/BF00232256.
Leadbetter, M.R., 1991. On a basis for "peaks over threshold" modeling. Stat. Prob. Lett. 12, 357–362.
Li, C., 2013. Subtidal water flux through a multiple-inlet system: observations before and during a cold front event and numerical experiments. J. Geophys. Res. Oceans 118, 1877–1892. https://doi.org/10.1002/jgrc.20149.
Lorenz, E.N., 1956. Empirical orthogonal functions and statistical weather prediction. In: Sci. Rep. No. 1. Statist. Forecasting Proj., Dept. Meteor, MIT, p. 49.
Matsoukis, C., Amoudry, L.O., Bricheno, L., et al., 2021. Investigation of spatial and temporal salinity distribution in a river dominated delta through idealized numerical modelling. Estuar. Coasts. https://doi.org/10.1007/s12237-021-00898-2.
Meier, H.E.M., 2007. Modeling the pathways and ages of inflowing salt and freshwater in the Baltic Sea. Estuar. Coast. Shelf S. 74, 610–627.
Monsen, N.E., Cloern, J.E., Lucas, L.V., Monismith, S.G., 2002. A comment on the use of flushing time, residence time, and age as transport time scales. Limnol. Oceanogr. 47, 1545–1553.
Newman, M., Sardeshmukh, P.D., 1995. A caveat concerning singular value decomposition. J. Clim. 8, 352–360.
Nixon, S.W., Ammerman, J.W., Atkinson, L.P., Berounsky, V.M., et al., 1996. The fate of nitrogen and phosphorus at the land-sea margin of the North Atlantic Ocean. Biogeochemistry 35, 141–180.
Nowacki, D.J., Ganju, N.K., 2018. Storm impacts on hydrodynamics and suspended-sediment fluxes in a microtidal back-barrier estuary. Mar. Geol. 404, 1–14. https://doi.org/10.1016/j.margeo.2018.06.016.
Officer, C.B., 1976. Physical Oceanography of Estuaries. Wiley, New York, New York, USA.
Oudijk, E., 2021. Short- and Long-Term Effects of Freshwater Discharge on Sea-Level Variability in back-Barrier Estuaries. Eindhoven University of Technology (TU/e), Eindhoven, the Netherlands.
Pannozzo, N., Leonardi, N., Carnacina, I., Smedley, R., 2021. Salt marsh resilience to sea-level rise and increased storm intensity. Geomorphology 389, 107825. https://doi.org/10.1016/j.geomorph.2021.107825.
Phelps, J.J., Polton, J.A., Souza, A.J., Robinson, L.A., 2013. Hydrodynamic timescales in a hyper-tidal region of freshwater influence. Cont. Shelf Res. 63, 13–22.
Philippart, C.J.M., Beukema, J.J., Cadée, G.C., Dekker, R., Goedhart, P.W., van Iperen, J. M., Leopold, M.F., Herman, P.M.J., 2007. Impacts of nutrient reduction on coastal communities. Ecosystems 10, 96–119.
Postma, H., 1950. The distribution of temperature and salinity in the Wadden Sea. Tijdschrift van het Koninkijk Nederlandsch Aardrijkskundig Genootschap 67, 34–42.
Ridderinkhof, H., 1988. Tidal and residual flows in the western Dutch Wadden Sea I: numerical model results. Neth. J. Sea Res. 22, 1–21.
Ridderinkhof, H., Zimmerman, J.F.T., 1990. Tidal exchange between the North Sea and Dutch Wadden Sea and mixing time scales of the tidal basins. Neth. J. Sea Res. 25, 331–350.
Schwichtenberg, F., Callies, U., van Beusekom, J.E.E., 2017. Residence times in shallow waters help explain regional differences in Wadden Sea eutrophication. Geo-Mar. Lett. 37, 171–177.
Smith, N., 1990. Wind Domination of Residual Tidal Transport in a Coastal Lagoon. Springer, New York, pp. 123–133.
Solari, S., Losada, M.A., 2012. A unified statistical model for hydrological variables including the selection of threshold for the peak over threshold method. Water Resour. Res. 48, W10541.
Takeoka, H., 1984. Fundamental concepts of exchange and transport time scales in a coastal sea. Cont. Shelf Res. 3 (3), 311–326.
Talke, S.A., de Swart, H.E., Schuttelaars, H.M., 2009. Feedback between residual circulations and sediment distribution in highly turbid estuaries: an analytical model. Cont. Shelf Res. 29, 119e135.
Valentine, K., Mariotti, G., 2019. Wind-driven water level fluctuations drive marsh edge erosion variability in microtidal coastal bays. Cont. Shelf Res. 176, 76–89. https://doi.org/10.1016/j.csr.2019.03.002.
van de Kreeke, J., Cotter, D., 1974. Tide-induced mass transport in lagoon-inlet systems. Coast. Eng. 14, 2290–2301.
Zhang, W.G., Wilkin, J.L., Chant, R.J., 2009. Modeling the pathways and mean dynamics of river plume dispersal in the New York Bight. J. Phys. Oceanogr. 39, 1167–1183.
Zhang, J., Wang, P., Hughes, J., 2012. EOF analysis of water level variations for microtidal and mangrove-covered Frog Creek system, west-central Florida. J. Coast. Res. 28 (5), 1279–1288.
Zhang, X., Leonardi, N., Donatelli, C., Fagherazzi, S., 2020. Divergence of sediment fluxes triggered by sea level rise will reshape coastal bays. Geophys. Res. Lett. https://doi.org/10.1029/2020GL087962.
Zimmerman, J.T.F., 1976. Mixing and flushing of tidal embayments in the western Dutch Wadden Sea. Part I: distribution of salinity and calculation of mixing time scales. Neth. J. Sea Res. 10 (2), 149–191. https://doi.org/10.1016/0077-7579(76)90013-2.
Zimmerman, J.T.F., 1981. Dynamics, diffusion and geomorphological significance of tidal residual eddies. Nature 209, 549–555.